Effects of long-term treatment of denosumab on bone mineral density: insights from an in-silico model of bone mineralization

Javier Martínez-Reina[a,1,*], Peter Pivonka[b,2]

[a] *Departmento de Ingeniería Mecánica y Fabricación, Universidad de Sevilla, Seville 41092, Spain*
[b] *School of Chemistry, Physics and Mechanical Engineering, Queensland University of Technology, QLD 4000, Australia.*

Abstract

Denosumab is one of the most commonly prescribed anti-resorptive drugs for the treatment of postmenopausal osteoporosis. The therapeutic effect of denosumab is to inhibit osteoclast differentiation and consequently bone resorption. Gains in bone mineral density (BMD) are achieved based on the ability of the bone matrix to undergo secondary mineralization. Experimental data show that the increase of BMD after commencing denosumab treatment are bone site specific.

In this paper, we developed a comprehensive mechanistic pharmacokinetic-pharmacodymamic (PK-PD) model of the effect of denosumab on bone remodeling in postmenopausal osteoporosis (PMO). The PD model is based on a bone cell population model describing the bone remodeling process at the tissue scale. The conceptual model of the bone mineralization process, originally proposed by Boivin and Meunier, is quantitatively incorporated using a FIFO (First-In-First-Out) queue algorithm. The latter takes into account the balance of mineral within bone tissue due to the mineralization process, distinguishing the primary and secondary phases and removal of bone matrix

*Corresponding author
[1] Departmento de Ingeniería Mecánica y Fabricación, Universidad de Sevilla. Escuela Técnica Superior de Ingeniería. Camino de los Descrubrimientos s/n, 41092. Sevilla. jmreina@us.es
[2] School of Chemistry, Physics and Mechanical Engineering, Queensland University of Technology, 2 George Street, Brisbane QLD 4000, Australia

due to bone resorption. The numerical simulations show that the model is able to predict the bone-site specific increase in BMD as was observed in the experimental data of Bone et al. 2008 for a typical denosumab administration pattern of 60 mg every 6 months. At the hip a 5 % increase in BMD was observed, while at the lumbar spine a 7.5 % increase of BMD was achieved after a 2 year treatment period. The difference in BMD is due to the fact that bone turnover at the hip is lower compared to lumbar spine and consequently has less potential for secondary mineralization. Parametric studies revealed that the rate of bone mineralization is an essential parameter regulating BMD gains. If mineralization is neglected only minimal increases in BMD are observed.

Keywords: postmenopausal osteoporosis; bone remodeling; bone mineralization; denosumab; RANK-RANKL-OPG pathway; PK-PD modeling; bone mineral density;

1. Introduction

Osteoporosis is a major skeletal disease linked to an imbalance in bone remodeling, with bone resorption exceeding bone formation [1]. This results in continuous bone loss and deterioration of the bone microarchitecture, which ultimately leads to impaired bone strength and increased risk of bone fracture [2][3]. Postmenopausal osteoporosis (PMO) has been linked to a decrease in estrogen production in mid-age women. The rate of bone loss is relatively high in the first year following menopause and then follows a linear pattern of approximately 1% bone loss per year [4][5]. Fractures related to osteoporosis are a major global health concern. With the increasing elderly population in first world countries, the risk of fracture is estimated to significantly increase over the next few years. In order to counteract this trend, a number of so-called anti-resorptive therapies have been developed including bisphosphonates and denosumab [6]. These therapies decrease osteoclastic bone resorption and have been shown to decrease the risk of osteoporotic fractures in PMO [2]).

Denosumab is one of the most commonly prescribed anti-resorptive drugs for the treatment of PMO [2]. The therapeutic effect of denosumab is based on its ability to inhibit osteoclast formation and activity. The FREEDOM study indicates that after 3 years of denosumab treatment the incidence of new morphometric vertebral fractures decreased from 7.2% with placebo to

2.3% with denosumab (68% relative reduction)[2]. Short-term treatment (i.e. Phase 2 study) of PMO with denosumab has been shown to reduce relative risk of hip fractures by 40% and non-vertebral fractures by 20%. These clinical results clearly indicate high efficacy of denosumab for treatment of PMO. The therapeutic effects of denosumab can be monitored by looking at a variety of bone biomarkers including non-specific (i.e., blood or urine based) markers such as NTx, uTX, PICP/PINP and specific biomarkers, i.e. measured at a particular bone site such as bone mineral density (BMD) [4]. BMD is most commonly assessed at the femoral neck, wrist and vertebrae and it has been shown that denosumab has different effects on BMD depending on the bone site [4]. Largest increases in BMD are observed at bone sites exhibiting high bone turnover rate, while more moderate increases are observed at sites of lower turnover rate [3].

These experimental findings can be explained based on the conceptual model of bone mineralization, which links the rate of bone remodeling with the degree of bone tissue mineralization (BTM) [7][8]. Bone mineralization is characterized by a fast primary phase, which takes place over several days to weeks and achieves a degree of mineralization of approximately 70%, followed by a slow secondary phase, which can take from months to years and may achieve degrees of mineralization of up to 95%. This conceptual model states that bone sites undergoing high turnover are characterized by a lower BTM (and BMD) based on the fact that continuous remodeling prevents excessive secondary mineralization to occur. On the contrary, at sites of low turnover there is sufficient time for secondary mineralization to occur. Consequently, based on the fact that denosumab significantly reduces bone turnover due to inhibition of osteoclast activity, the treatment effects are more pronounced at bone sites exhibiting higher bone turnover [8].

The time dependent dose-effect response of drugs is most commonly described using pharmacokinetics (PK) − pharmacodynamics (PD) modeling approaches [9]. Among these, mechanistic PK−PD models allow taking into account organ-specific signaling pathways and regulatory mechanisms [4]. A variety of different mechanistic PK−PD models describing the bone remodeling process have been developed [10][11][12]. The majority of these models are based on the fundamental models of bone cell interactions in bone remodeling proposed by Lemaire et al (2004)[13] and Pivonka et al. (2008)[14]. These models incorporate the RANK-RANKL-OPG signaling pathway together with action of TGF$-\beta$ on bone cells. Particularly, the models of Pivonka et al. also provide a mechanistic description of changes in bone

porosity and bone volume faction (BV/TV) which are linked to bone cell numbers [14][15][12]. These bone cell population models provide a mechanistic means on how to link the action of denosumab to the bone remodeling process based on competitive binding reactions between OPG, denosumab and RANKL. Several authors have utilized this approach in different ways [10][11][16][12]. However, none of these models included a mechanistic description of the mineralization process.

In the present paper, we present a comprehensive mechanistic PK−PD model for quantifying the effect of denosumab on bone turnover and BMD taking into account the mineralization process. This model is an extension of a previously developed model of bone remodeling taking into account the process of bone mineralization. The bone remodeling model accounts for bone cell interactions via the RANK-RANKL-OPG pathway, the action of TGF$-\beta$ and mechanobiological feedback [14][15][12]. The PK model of denosumab is a one-compartment model including a drug saturation term for high doses and has been previously described by Marathe et al. 2011 [11]. The mineralization model is based on the work of Martí-Reina and co-workers [17] and takes into account the balance of mineral within bone tissue: input, due to the mineralization process, distinguishing the primary and secondary phases; removal, due to bone resorption, that takes mineral back into the blood serum.

Utilizing this model, we investigate some model features in a drug treatment scenario whose clinical results were available in the literature [18]. This includes the following parametric studies: taking or not taking into account the bone mineralization process and its effect on BMD; different drug distribution factors accounting for ease of accessibility of denosumab from the central compartment to the bone tissue compartment; and different bone sites undergoing high and low turnover. Based on the proposed mechanistic PK−PD model we are showing temporal evolution of bone biomarkers for these cases including bone porosity, BMD and the degree of mineralization.

This paper is organized as follows: In Section 2 we provide a detailed description of the mechanistic PK−PD model. The comparison of simulation results and experimentally observed changes in BMD are reported in Section 3, together with parametric studies of essential model parameters. The results are discussed in detail with respect to the clinical bone biology literature in Section 4.

2. Mechanistic PK-PD model for simulation of the effect of denosumab on bone remodeling

2.1. One compartment PK model of denosumab

Several pharmacokinetic (PK) models of denosumab have been proposed including one- and two-compartment models [19]. We here follow the approach suggested by Marathe et al. and use a one-compartment model with Michaelis-Menten kinetics in order to characterize the serum denosumab PK profiles. A first-order rate process (k_a) governs the absorption of drug ($Dose_{den}$) from the subcutaneous (SC) injection site into the central compartment ($C_{P,den}$, V_c). The drug elimination from the central compartment is described by a combination of a linear first-order process (k_{el}) and a nonlinear saturation process (V_{max} , K_m)[11]:

$$\frac{dC_{p,den}}{dt} = k_a \frac{Dose_{den}}{V_c/F} \cdot e^{-k_a\, t} - \frac{C_{p,den}}{K_m + C_{p,den}} \frac{V_{max}}{V_c/F} - k_{el} \cdot C_{p,den} \qquad (1)$$

where, V_c/F is the volume of the central compartment adjusted for bioavailability. In Eq. (1) $Dose_{den}$ is given in ng per kg of body weight and then $C_{p,den}$ is calculated in ng/ml and subsequently converted into pmol/l, through the molecular weight of denosumab $M_{den} = 149$ kDa (Amgen) and using principles of physical chemistry. We note that all ligand receptor binding reactions presented in the following sections are formulated with units pmol/l. Note that V_c is the volume of the central compartment and the factor F is the bioavailability. The latter factor is equal to 1 when the drug is administered intravenously. The initial condition for Eq.(1) is set to zero, indicating absence of drug. The prolonged absorption phase and the absence of intravenous data precludes the need for including distribution of the drug to a non-specific tissue compartment and thus reduces the number of parameters in this model. Table 2 in the Appendix summarises the PK model parameters.

2.2. Model of bone cell interactions in bone remodeling

In the following, a description of the extended mathematical model describing bone cell interactions taking into account bone mineralization is provided. Similar as in previous models, the RANK-RANKL-OPG pathway, together with the action of several regulatory factors on bone cells, including TGF$-\beta$, and mechanobiological feedback is given (for details on original models see Pivonka et al. [14][15][20]. This new model has been designed in

such a way that the original model structure has been preserved and only additional model features relevant to formulation of the mineralization law have been taken into account.

Following the approach taken by Pivonka et al., the bone remodeling process can be described as cell balance equations. The bone cell types (i.e. state variables) considered in the current model are: (i) osteoblast precursor cells (OB_p), (ii) active osteoblasts (OB_a), and active osteoclasts (OC_a). The cell pools of uncommitted osteoblasts (OB_u) and osteoclast precursors (OC_p) are assumed constant:

$$\begin{aligned}\frac{dOB_p}{dt} &= D_{OB_u}\cdot\pi^{TGF-\beta}_{act,OBu}\cdot OB_u + P_{OB_p}\cdot\Pi^{mech}_{act,OB_p}\cdot OB_p + \\ &\quad - D_{OB_p}\cdot\pi^{TGF-\beta}_{rep,OB_p}\cdot OB_p;\end{aligned} \tag{2}$$

$$\frac{dOB_a}{dt} = D_{OB_p}\cdot\pi^{TGF-\beta}_{rep,OB_p}\cdot OB_p - A_{OB_a}\cdot OB_a; \tag{3}$$

$$\frac{dOC_a}{dt} = D_{OC_p}\cdot\pi^{RANKL}_{act,OC_p}\cdot OC_p - A_{OC_a}\cdot\pi^{TGF-\beta}_{act,OC_p}\cdot OC_a; \tag{4}$$

D_{OB_u}, D_{OB_p}, D_{OC_p} are differentiation rates of $\mathrm{OB_u}$, $\mathrm{OB_p}$ and $\mathrm{OC_p}$ respectively. P_{OB_p} is the proliferation rate of $\mathrm{OB_p}$. A_{OB_a} and A_{OC_a} are apoptosis rates of $\mathrm{OB_a}$ and $\mathrm{OC_a}$ respectively. The variables $\pi^{TGF-\beta}_{act,OBu}$, $\pi^{TGF-\beta}_{rep,OB_p}$ and $\pi^{TGF-\beta}_{act,OC_p}$ represent activator and repressor functions related to the binding of TGF-β to its receptor. Similarly, π^{RANKL}_{act,OC_p} is the activator function related to the RANK-RANKL binding. Π^{mech}_{act,OB_p} is the mechanobiological feedback function regulating the anabolic part of the feedback. We note that the cell balance equations (Eq.2-4) are composed of a production term and a linear degradation term, which describes differentiation of one cell type into another (or terminal cell fate, i.e. apoptosis). The linear degradation term is further regulated via sigmoidal activator/repressor functions which take values from zero to one. The latter functions introduce nonlinearities into the model. A schematic figure of the mechanistic PK-PD model is presented in Fig. 1. Model parameters of the cell population model are given in Table 2 of the Appendix.

2.3. Denosumab action on RANK-RANKL-OPG: competitive binding

Similar to previous mechanistic PK-PD models, we incorporate the action of denosumab on bone remodeling via competitive binding reactions

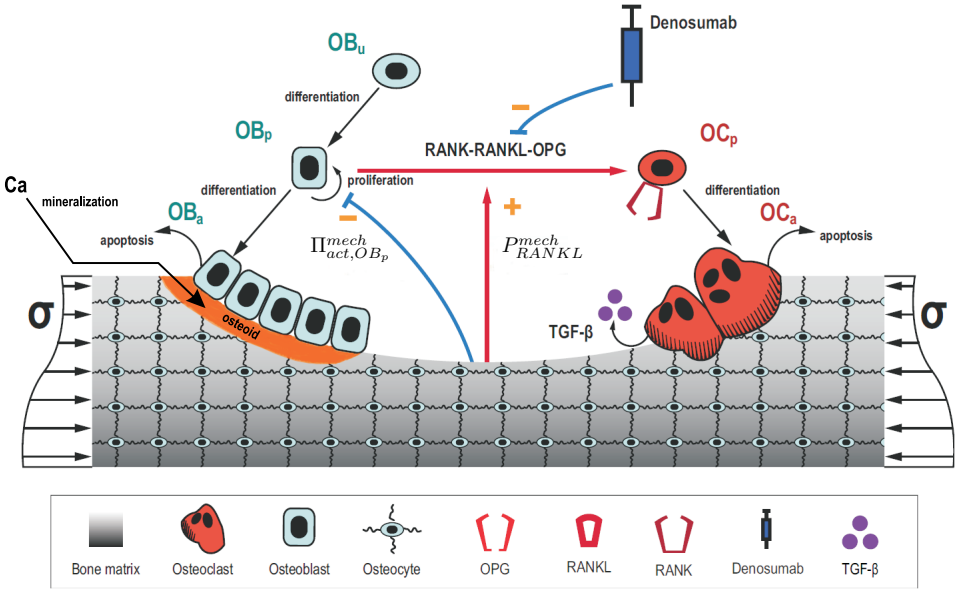

Figure 1: Schematic representation of the mechanistic PK-PD model: various bone cell differentiation stages are presented together with biochemical and biomechanical interactions. Subcutaneous injection of densumab leads to distribution of the drug into the central compartment where it then interacts with the RANK-RANKL-OPG pathway (red arrow between OB_p and OC_p). The latter interactions are accounted for via competitive binding reactions. Also the conversion of osteoid into bone mineral, the major novel model feature, is shown in orange in the figure.

within the RANK-RANK-OPG pathway [10][11][12]. In these models action of denosumab is taken into account via the RANKL activator function π_{act,OC_p}^{RANKL} (Eq(4), first term on the right). Denosumab competes with RANK (and OPG) for binding to RANKL. Consequently, higher concentrations of denosumab give rise to lower concentrations of RANKL-RANK complexes and, hence, lower values of π_{act,OC_p}^{RANKL}. Adapting the approach of Pivonka et al. [12],

$$\mathrm{RANKL} = \mathrm{RANKL}^{\max}\frac{\beta_{\mathrm{RANKL}} + P_{\mathrm{RANKL}}}{\beta_{\mathrm{RANKL}} + \tilde{D}_{\mathrm{RANKL}}\mathrm{RANKL}^{\max}}\cdot$$
$$\cdot\left[1 + K_{\mathrm{a,[RANKL\text{-}OPG]}}\mathrm{OPG} + K_{\mathrm{a,[RANKL\text{-}RANK]}}\mathrm{RANK} + \zeta K_{\mathrm{a,[RANKL\text{-}den]}}C_{p,den}\right]; \tag{5}$$

where $K_{\mathrm{a,[RANKL\text{-}OPG]}}$, $K_{\mathrm{a,[RANKL\text{-}RANK]}}$, and $K_{\mathrm{a,[RANKL\text{-}den]}}$ are the equilibrium association binding constants for binding of OPG, RANK and denosumab to RANKL. OPG, RANK, and RANKL are the concentrations of respective regulatory factors in the bone tissue compartment, while $C_{p,den}$is the concentration of denosumab in the central compartment (see Eq.(1)) [3]. β_{RANKL} is the production rate of RANKL on the surface of osteoblasts, $\tilde{D}_{\mathrm{RANKL}}$ is the RANKL degradation rate, $\mathrm{RANKL}^{\max}$ is the maximum concentration of RANKL and P_{RANKL} models the increase in RANKL production induced by PMO. Model parameters for the competitive binding model are given in Table 2.

In Eq.(5) all association binding constants K_a are obtained from in vitro experiments. Furthermore, RANKL production and degradation rate constants were estimated from previous works (see Table 2). Hence, the only remaining factor to estimate was the accessibility factor ζ. The varying accessibility of denosumab to different bone tissue compartments is taken into account through the accessibility factor ζ. $\zeta = 1$ represents unrestricted access to denosumab, whereas $\zeta < 1$ reflects restricted access (for example due to bone marrow being present or low blood perfusion). Hence, the denosumab concentration is bone site specific. In the numerical results section we will perform a parametric study to quantify appropriate values for ζ, which

[3]Note that in the original Lemaire et al. model [13] all concentrations where formulated with respect to a pseudo central compartment and consequently no distinction between site-specific bone tissue compartments needs to be made. However, formulation of mechanobiological PK-PD models requires specification of a particular bone site which is exposed to physiological mechanical loading.

will eventually act as a calibration factor. Finally, the activator function of RANKL can be expressed as:

$$\pi_{act,OC_p}^{RANKL} = \frac{[\text{RANKL-RANK}]}{K_{\text{d,[RANKL-RANK]}} + [\text{RANKL-RANK}]}; \tag{6}$$

with $K_{\text{d,[RANKL-RANK]}}$ as the corresponding equilibrium dissociation binding constant. Model parameters of the binding reactions are provided in Table 2 in the Appendix.

2.4. Algorithm of bone mineralization

Bone is a composite of tissue matrix and pores, which may be filled with marrow, blood vessels and nerves. A reference bone volume, V_{RVE}, can be divided into the bone matrix volume, V_{bm}, and the volume of vascular pores, V_{vas}. Bone matrix is composed of an inorganic phase (mineral), an organic phase (mainly collagen) and water. The volume of each phase are designated by V_m, V_o and V_w, respectively:

$$V_{RVE} = V_{bm} + V_{vas} = V_m + V_o + V_w + V_{vas} \tag{7}$$

The link between the bone cell population model described in Section (2.2) and bone mechanical properties can be made using the approach taken by Pivonka and co-workers [20, 21]. In this approach, activities of osteoblasts and osteoclasts define the evolution of the volume fraction of extravascular bone matrix f_{bm}. The latter is defined as follows: $f_{bm} = V_{bm}/V_{RVE}$, whereas the volume fraction of vascular pores is defined as the volume of pores divided by the total RVE volume, i.e., $f_{vas} = V_{vas}/V_{RVE}$ with the constraint $f_{bm} + f_{vas} = 1$. The change of bone volume fraction over time is defined by the balance of bone removed and formed:

$$\frac{df_{bm}}{dt} = -k_{res} \cdot OC_a + k_{form} \cdot OB_a; \tag{8}$$

where k_{res} and k_{form} are respectively the bone matrix volume resorption rate and osteoid volume formation rate. This distinction is important since bone matrix is mineralized, while osteoid contains no mineral. OC_a and OB_a are the concentrations of OC_a and OB_a, respectively defined in Eq(3) and (4). Note that, as a first approximation, we assume that k_{res} and k_{form} are constant cell intrinsic parameters. The set of differential equations (2),(3),(4),(8) were integrated using an explicit Euler algorithm, coded

in MATLAB R2017a. Concentrations of regulatory factors, cell populations and bone volume fraction are positive quantities and so they were forced to be during the integration of equations. The integration time step was fixed at 0.25 days after performing a convergence analysis, in which this value was proven to be small enough to get stable and consistent solutions.

The osteoid laid *de novo* by osteoblasts consists only of organic phase and water. Some of this water is later replaced with mineral, during the mineralization process. This process has three phases: an initial phase, called mineralization lag time, that takes from 6 to 22 days [22, 23] during which no deposition of mineral occurs; a primary phase, very quick (it takes a few days to reach the 70% of the maximum mineral content [24]), and a secondary phase, when mineral is added at an exponentially decreasing rate [25], as the tissue becomes saturated with mineral and which may last from 6 months [26] to several years [27].

The mineral content is usually measured by the so-called ash fraction, defined as the ratio between mass of mineral m_m (also termed ash mass) and dry mass (the sum of mineral and organic mass):

$$\alpha = \frac{m_m}{m_m + m_o} = \frac{\rho_m V_m}{\rho_m V_m + \rho_o V_o} \tag{9}$$

where the densities of the mineral and organic components are respectively $\rho_m = 3.2\, g/cm^3$ and $\rho_o = 1.1\, g/cm^3$ [28].

We define the specific volumes $v_o = V_o/V_b$, $v_m = V_m/V_b$ and $v_w = V_w/V_b$ (then $v_o + v_w + v_m = 1$ holds). Equation (9) can be given in terms of specific volumes, dividing by V_b, and hence:

$$\alpha = \frac{\rho_m\, v_m}{\rho_m\, v_m + \rho_o\, v_o} \tag{10}$$

Bone apparent density can be assessed through:

$$\rho = \rho_m\, v_m + \rho_o\, v_o + \rho_w\, v_w \tag{11}$$

Mineral accumulates by displacing water present in bone matrix [24]. For this reason, the volume ratio of organic phase would be constant during the mineralization process, around $v_o = 3/7$ [29], which was assumed a fixed value; while the variations of mineral and water volume ratios would hold $\Delta v_m = -\Delta v_w$.

We have assumed that v_m increases with time following Eq. (12) (based on [24]), which distinguishes the mineralization lag time; the primary phase,

with a linear increase and the secondary phase, with an exponentially decreasing rate:

$$v_m(t) = \begin{cases} 0 & \text{if} \quad t \leq t_{mlt} \\ v_{m\,prim}\,\dfrac{t - t_{mlt}}{t_{prim}} & \text{if} \quad t_{mlt} < t \leq t_{prim} + t_{mlt} \\ v_{m\,max} - (v_{max} - v_{prim})\,e^{-\kappa\cdot(t - t_{prim} - t_{mlt})} & \text{if} \quad t_{prim} + t_{mlt} < t \end{cases} \tag{12}$$

where t_{mlt} and t_{prim} are the length of mineralization lag time and primary phase respectively; $v_{m\,prim}$ is the mineral specific volume at the end of the primary phase, corresponding to $\alpha = 0.45$ [24]; $v_{m\,max}$ is the mineral specific volume corresponding to the maximum calcium content, $300\,mg/g$ [28]; and finally, κ is a parameter measuring the rate of mineral deposition during the secondary phase (see Table 1). Only continuity is enforced in equation (12). Differentiability is not needed since the set of differential equations were integrated using an Euler explicit algorithm, as stated above.

The amount of mineral contained in a RVE depends on the age of the tissue through Eq. (12), but the RVE can be made up of patches of tissue that have been formed in the recent history, viz. of different ages. It must be taken into account as well that the tissue within the RVE can be resorbed, so taking the mineral back into the blood flow. The amounts of tissue with different ages contained in the RVE are estimated using the algorithm first presented in [17] and depicted in Fig. 2. $\overline{V}_{form}(t,\tau)$ is defined as the bone volume formed τ days ago and still present (not resorbed) at time t. Then, knowing the distribution of tissue patches of different ages at day t (left column) and the volume formed ($V_{form}(t) = k_{form}\,OB_a(t)$) and resorbed that day ($V_{res}(t) = k_{res}\,OC_a(t)$), the distribution at day $t+1$ (right column) can be estimated, using:

$$\overline{V}_{form}(t+1, i+1) = \overline{V}_{form}(t,i) - V_{res}(t)\,\frac{\overline{V}_{form}(t,i)}{V_b(t)} \tag{13}$$

The second term of the right-hand side represents the fraction of volume $\overline{V}_{form}(t,i)$ which is resorbed at day t. It is assumed that the tissue volume formed in previous days is uniformly distributed throughout the RVE. Consequently, that fraction is proportional to the concentration $\frac{\overline{V}_{form}(t,i)}{V_b(t)}$, and to the resorbed volume, $V_{res}(t)$.

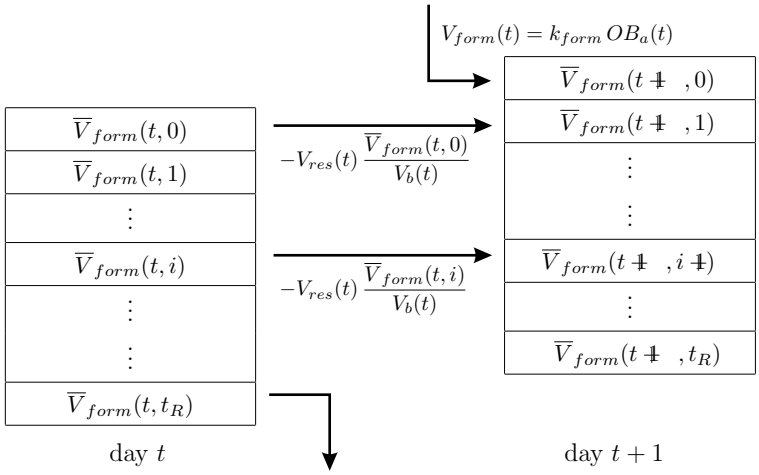

Figure 2: FIFO queue algorithm used to update the distribution of tissue patches of different ages within the RVE.

The queue is truncated at the residence time, t_R, the typical time the tissue patches remain in the RVE before being totally resorbed. In other words, t_R is the first day such that $\overline{V}_{form}(t, t_R + 1) = 0$ and depends on the turnover rate. Then,

$$V_b(t) = \sum_{i=0}^{t_R} \overline{V}_{form}(t, i) \tag{14}$$

must hold. Formally, in the algorithm of Fig. 2, $t_R \to \infty$, but, for normal turnover rates, the older elements are negligible and the queue can be truncated at day $i = t_C$ ($t_C < t_R$). Thus, it can be assumed that $\overline{V}_{form}(t, i) \sim 0 \quad \forall\ i > t_C$. The parameter t_C was limited to 1000 days to reduce the computational cost. By doing so, there is a residual old tissue:

$$V_{residual}(t) = V_b(t) - \sum_{i=0}^{t_C} \overline{V}_{form}(t, i) \tag{15}$$

and now Eq. (14) holds by replacing t_R with t_C only if this residual old tissue is added. Finally, the mineral content of each patch is summed to estimate

the average mineral content of the RVE at day $t+1$.

$$v_m(t+1) = \frac{\sum_{i=0}^{t_C} \overline{V}_{form}(t+1,i) \cdot v_m(i) + V_{residual}(t+1) \cdot v_{m\,max}}{V_b(t+1)} \tag{16}$$

where the mineral contents of the patches, $v_m(i)$, are calculated through Eq. (12) and $V_{residual}$ has been assumed to contain the maximum mineral content $v_{m\,max}$.

Parameter	Description	Nominal value	Other examined values	Units
t_{mlt}	Mineralization lag time	$12^{a,b}$		days
t_{prim}	Length of primary phase	10^{c}		days
$v_{m\,prim}$	v_m at the end of primary phase	0.121		-
$v_{m\,max}$	Maximum mineral specific volume	0.442		-
κ	Rate of secondary phase	0.007	0.001, 0.003, 0.005, 0.009	-

Table 1: Parameters of the mineralization model. [a] Brockstedt et al. (1993), [b] Parfitt (2004), [c] Hernandez et al. (2001)

The mineral content has influence on the mechanical properties, and particularly on the stiffness of bone tissue, which was studied by Hernandez et al. [30]. We have assumed that bone tissue is isotropic with a Young's modulus given by the correlation obtained experimentally by those authors:

$$E(\text{MPa}) = 84370\, f_{bm}^{2.58}\, \alpha^{2.74} \tag{17}$$

A constant, uniaxial compressive stress $\sigma = 5\,MPa$ was applied on the trabecular bone. This value together with the Young's modulus given in Eq. (17) allows calculating the strain energy density, Ψ. The latter quantity is used as a mechanoregulatory feedback stimulus acting anabolically via Π_{act,OB_p}^{mech} and catabolically via π_{act,OC_p}^{RANKL} (see Scheiner at al [20] for details). Note that in the current model, mechanical properties vary not only with the porosity but also with the mineral content.

3. Results

We follow the approach described in detail in Lemaire et al. [13] and Pivonka et al. [14][15] to simulate disease progression in PMO with subsequent denosumab treatment. The following biomarkers are investigated:

bone cell numbers and BMD. While the former are representative for non-specific bone resorption and formation markers, the latter are bone specific and reflects the material properties.

PMO was simulated by introducing a disease-related increase in RANKL production over time [12]:

$$P_{\mathrm{RANKL}}(t) = P_{\mathrm{RANKL}}^{\mathrm{PMO,ini}}\ \varphi_{\mathrm{PMO}}^{\mathrm{RANKL}}(t) \tag{18}$$

where $P_{\mathrm{RANKL}}^{\mathrm{PMO,ini}} = 4 \cdot 10^3\,\mathrm{pM}$ and $\varphi_{\mathrm{PMO}}^{\mathrm{RANKL}}$ is a reduction factor defined as:

$$\varphi_{\mathrm{PMO}}^{\mathrm{RANKL}}(t)s = \frac{\xi^2}{\xi^2 + \left[\frac{t - t_{\mathrm{PMO,ini}}}{\tau_{\mathrm{PMO}}^{\mathrm{RANKL}}}\right]^2} \tag{19}$$

with $\xi = 65$ and $\tau_{PMO}^{RANKL} = 900$ days, being characteristic values and $t_{\mathrm{PMO,ini}}$ the disease onset time. One year of PMO was simulated prior to the beginning of the treatment, which consisted in subcutaneous injection of 60 mg of denosumab every 6 months, in accordance with the treatment analyzed in Bone et al. [31] and one of those analyzed in Miller [18].[4]

3.1. Parametric studies: bone site, bone turnover rate and drug distribution

The predicted evolution of apparent bone density is shown in Fig. 3 in a continuous manner. The onset of PMO leads to an initial significant bone loss which starts to slow down at the end of the first year [4] [5]. One year after the onset of the disease the denosumab treatment commences, with a sharp increase in bone density related to an increase in bone volume. This increase in bone volume is reduced later on and the observed increase in bone density is mostly due to the rise in mineral content. The oscillations observed in the evolution of bone density are due to the variable blood serum concentration of denosumab, which also oscillates strongly with injections every 6 months. Clearly, the model predicts an overall bone density gain with time.

For comparison purposes, the results were screened at 1, 6, 12 and 24 months, as is typically performed in clinical studies, including the one of Bone et al. [31]. These authors measured the bone density gain (BDG) with

[4] A body weight of 60 kg has been assumed to calculate $Dose_{den}$ in ng per kg of body weight.

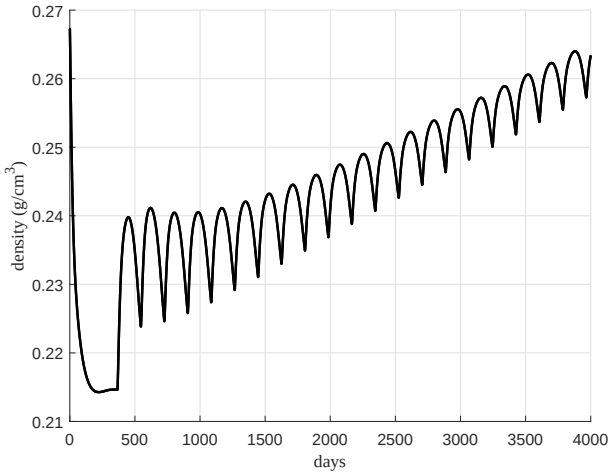

Figure 3: Evolution of apparent bone density for $f_{bm\,t0} = 15\%$ and $\zeta = 0.012$.

respect to baseline, the density measured at the beginning of treatment, i.e. after 1 year of PMO in the present simulations:

$$\mathrm{BDG}(\%) = \frac{\rho(t) - \rho(1\,year)}{\rho(1\,year)} \cdot 100 \tag{20}$$

BDG obtained here in silico was compared with the values reported in that clinical study so as to adjust the drug accessibility factor ζ. Fig. 4 compares the effect of ζ on BDG for a trabecular bone of high porosity ($f_{bm\,t0} = 15\%$), representative of vertebral bone. From the comparison of these simulation results with the clinical results of Bone et al. [31] it can be seen that $\zeta = 0.012$ provides the best approximation. This value will be used in all subsequent simulations. It can be seen that the numerical results predict an abnormally high BDG at the beginning of the treatment, which is influenced by the absorption term (k_a) of the PK model (see Eq. (1)), as will be discussed in the Appendix.

The next set of simulations investigates the effect on BDG of different initial porosities, which is representative for different bone sites such as vertebral body/Lumbar spine and femoral neck/Hip. Fig. 5 compares the simulation results with the clinical data of Bone et al. [31] for different initial porosities $f_{bm\,t0}$. This figure shows that bone sites with smaller $f_{bm\,t0}$ exhibit a larger increase of BDG compared to bone sites with higher $f_{bm\,t0}$.

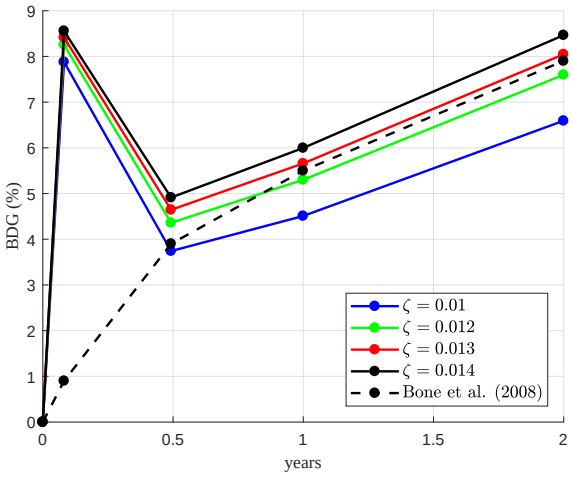

Figure 4: Influence of drug accessibility factor ζ on BDG (%) for $f_{bm\,t0} = 15\%$.

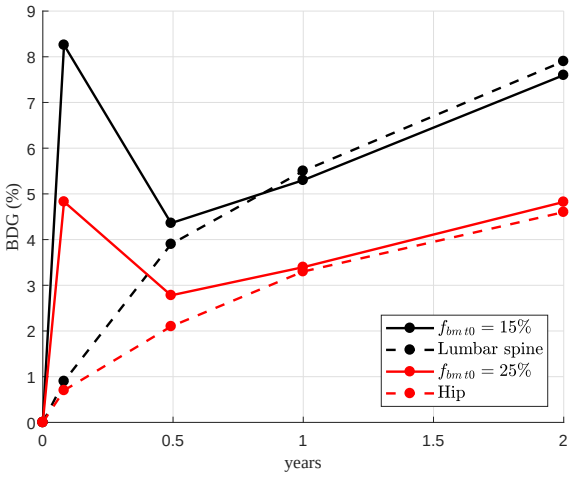

Figure 5: Influence of initial bone volume fraction, $f_{bm\,t0}$, on BDG. Only BDG measured at 1, 6, 12 and 24 months are presented according to data in Bone et al. [31]

.

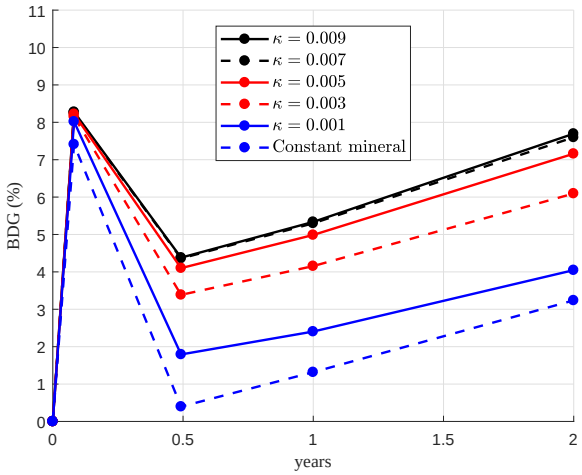

Figure 6: Influence of the bone mineralization rate on BDG.

The effect of the mineralization rate on BDG is analyzed in Fig. 6 through the parameter κ, which measures the rate of mineral deposition during the secondary phase of mineralization. During this phase the tissue accumulates mineral at a decreasing rate and it can take from 6 months [26] up to several years [27] to reach 95% of the maximum mineral content. In Eq. (12), $\kappa = 0.007$ corresponds to 6 months while $\kappa = 0.001$ corresponds to 4 years. It can be seen that a lower mineralization rate (i.e., a smaller κ value) makes the denosumab treatment less effective. Actually, changes in BDG are mostly due to the increase in mineral content, which is clearly seen in the case where the mineral content is assumed constant (see dashed blue curve). Here, the increase in apparent density is only due to the decrease in porosity and is very limited and not in accordance with the clinical results. However, when the variation in mineral content is considered, inhibition of bone turnover leads to an increase in the mineral content of the existing bone tissue and consequently in bone density. Moreover, for $\kappa = 0.007$ bone tissue gets saturated with mineral quite quickly and further increases in κ have no noticeable influence (black dashed and solid curves are almost coincident).

The final set of simulations investigates the effect of bone turnover rate (Fig. 7) for different initial bone matrix volume fractions ($f_{bm\,t0}$). The normal turnover rate k_{res} was multiplied by 2 and 0.5 to analyze high and low turnover rates, respectively. These simulations test the conceptual miner-

alization model proposed by Boivin and Meunier [7][8], which predicts that bone tissue undergoing high turnover will exhibit a higher change in bone tissue density compared to bone sites with lower bone turnover once remodeling is inhibited with anti-resorptive agents. Indeed all simulations confirm that the average slope ($\Delta\rho/\Delta t$) of changes in bone tissue density is larger for high bone turnover sites (dashed lines) compared to low bone turnover sites (dotted lines) with sites of normal turnover exhibiting an intermediate slope (see Fig. 7). The slope for $k_{res}X2$ is approximately 43% higher than the slope for the nominal value, k_{res}, and this is 92% higher than the slope for $k_{res}X0.5$. No noticeable differences were found between the slopes for different $f_{bm\,t0}$. Thus, the different BDG observed in Fig. 5 can only be explained by the reference density used to define BDG ($\rho(1year)$), which is different for each $f_{bm\,t0}$. In other words, BDG is greater for less dense bone sites only in relative terms.

4. Discussion

In this paper we presented a novel mechanistic PK-PD model describing the effect of the anti-catabolic drug denosumab on bone remodeling and the associated changes in bone mineral density. Unlike for anabolic drugs, where bone volume (and consequently bone mineral density) is gained due to bone formation by osteoblasts, for anti-catabolic drugs the existing bone matrix has the ability to embed more mineral in the extrafibrillar space, so increasing bone tissue density. The latter phenomenon of bone mineralization is strongly influenced by the bone turnover rate, which in turn is defined by the activity of osteoclasts.

The conceptual model of bone mineralization was originally proposed by Boivin and Meunier and states that bone undergoing higher remodeling activity is less mineralized compared to bone that exhibits fewer remodeling events [7]. This is due to the fact that bone matrix undergoes mineralization until it is remodeled, when osteoclasts dissolve it, putting the mineral back in the marrow.

The proposed computational model clearly indicates that the phenomenon of bone mineralization is primarily responsible for the bone density gain after commencing denosumab treatment. More generally, this is true for any anti-resorptive drug treatment. Neglecting the ability of bone matrix to increase its mineral content delivers only moderate increase of BMD (see Fig. 6 “Constant mineral”). Our numerical simulation results indicate that pa-

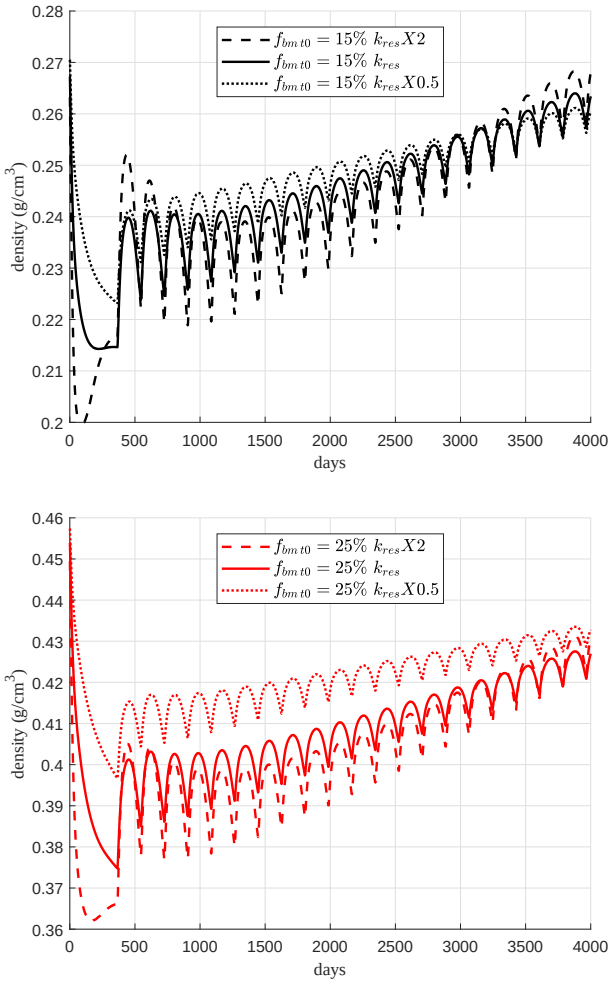

Figure 7: Influence of different bone turnover rates on BDG for different initial porosities.

tients with high bone turnover would respond more efficiently to treatments with anti-catabolic drugs than patients with low turnover.

We note that several PK-PD models have been presented decribing the effect of denosumab on BMD [10][11][16][12]. However, none of these models have included a consistent mechanistic description of the mineralization process. Simulation results of Scheiner et al. (2014) indicated that without incorporation of the mineralization process the significant increases in BMD during denosumab treatment could not be predicted based on suppression of osteoclast activity alone [12]. On the other hand, the model of Marathe et al. (2011) included a phenomenological equation for BMD which was constructed such that the experimental data could be well reproduced [11]. The work of Marathe et al. used a zero order degradation rate of BMD in order to adjust the slope of the BMD versus time curve [11]. The latter approach was phenomenological in nature and required additional fitting parameters to predict bone gains. Clearly, the formation of osteoid by active osteoblasts and subsequent mineralization of osteoid taking into account primary and secondary mineralization processes are a necessary prerequisite to accurately predict the action of denosumab on bone turnover and BMD.

As described in Peterson and Riggs, the lumbar spine BMD was predicted using a zero-order production rate that is affected by osteoblast function and a first-order elimination that is affected by osteoclast function. Sigmoidicity terms for each bone marker are estimated to describe the steepness of the BMD change relative to the proportional change in the marker [16]. As shown in our simulation results, the steepness of the BMD versus time curve (after administration of denosumab) is exclusively determined by the respective bone turnover rate. No additional model parameters are required to adjust/fit the slope of the BMD curve.

One issue to be addressed in the future is the fact that a highly mineralized bone matrix gives rise to a more brittle material behavior, which increases the stiffness and reduces the fracture toughness of bone [8]. The effects on bone stiffness and fracture toughness in combination with reduced bone remodeling during drug treatment is of major concern regarding development of fatigue damage. Hence, monitoring the degree of tissue mineralization is important and allows for designing patient-specific drug administration regimes including dose, administration interval and "drug holidays" which assure predefined bounds for the degree of bone mineralization [32][33][34].

5. Summary and conclusions

In this paper, a comprehensive mechanistic PK-PD model has been presented which allows simulating the effects of denosumab treatment on bone remodeling and bone mineral density (BMD) in postmenopausal osteoporosis. For this purpose, a PK model of denosumab has been coupled to a bone cell population model of bone remodeling taking into account the mineralization process. The latter accounts for the mineral balance in bone tissue and distinguishes between primary and secondary mineralization and removal of bone matrix due to bone resorption. Furthermore, mechanobiological feedback was accounted for in the model. The numerical simulation results have shown the following novel model capabilities:

- The bone mineralization process is an essential mechanism of bone mineral density (BMD) gains after treatment with denosumab. Neglecting bone mineralization (i.e. assuming a constant mineral content) leads to a significant reduction of BMD gains.

- The potential for mineralization is strongly affected by the rate of mineralization and consequently affects changes in BMD over time. High values of the mineralization rate lead to earlier saturation of the mineralization process.

- The initial bone turnover is an essential factor in determining bone's ability to continue the mineralization process upon reducing bone resorption due to anti-catabolic drug treatments. The slope of the BMD vs. time curves is increased for high bone turnover, while it is reduced for low turnover cases.

- The drug accessibility factor is an essential parameter which controls the ease by which denosumab is distributed from the central compartment to the respective bone tissue compartment.

- The effect of denosumab on BMD is bone site specific. The lumbar spine exhibits a higher bone turnover rate compared to the hip and, consequently, denosumab treatment is more effective in increasing BMD in the lumbar spine in relative terms.

We note that the current model does not include the formation of microcracks due to dynamic mechanical loading as occurs during habitual loading.

The increased brittleness of the bone matrix following denosumab treatment can be of concern for patients being on denosumab treatment for extended time periods. In future studies we aim to explore these effects in more detail identifying safe time periods for anti-resorptive treatments.

Appendix

The values of the constants of the PK-PD model are given in table 2. A detailed discussion of these values can be consulted in [11] and [12].

Parameter	Nominal value	Other examined values	Units
k_{res}	2	1, 4	pM^{-1} day^{-1}
k_{form}	0.4		pM^{-1} day^{-1}
D_{OB_u}	$7 \cdot 10^{-2}$		day^{-1}
D_{OB_p}	$1.657 \cdot 10^{-1}$		day^{-1}
D_{OC_p}	2.1		day^{-1}
A_{OB_a}	0.211		day^{-1}
A_{OC_a}	5.65		day^{-1}
β_{RANKL}	$1.684 \cdot 10^{2}$		pM day^{-1}
$\tilde{D}_{\text{RANKL}}$	$1.013 \cdot 10^{1}$		day^{-1}
ζ	0.012	0.01, 0.013, 0.014	-
$K_{\text{a,[RANKL-OPG]}}$	$1 \cdot 10^{-3}$		pM^{-1}
$K_{\text{a,[RANKL-RANK]}}$	$3.412 \cdot 10^{-2}$		pM^{-1}
$K_{\text{a,[RANKL-den]}}$	0.333		pM^{-1}
k_a	0.170	0.017	day^{-1}
k_{el}	$1.15 \cdot 10^{-2}$		day^{-1}
V_c	$7.79 \cdot 10^{1}$		ml kg^{-1}
F	1		-
K_m	$4.11 \cdot 10^{2}$		ng ml^{-1}
V_{max}	$2.672 \cdot 10^{3}$		ng kg^{-1} day^{-1}

Table 2: Values taken for the constants of the PK-PD model

We must note the influence of the absorption parameter of the PK model, k_a. In the paper, we have maintained the nominal value adjusted in [11], because its influence on the long-term results is almost negligible, but the short-term BDG is strongly affected by this absorption constant, as can be seen in Fig. 8, and should be investigated in the future.

References

[1] Bernabei, R., Martone, A.M., Ortolani, E., Landi, F., Marzetti, E.. Screening, diagnosis and treatment of osteoporosis: a brief review. Clin-

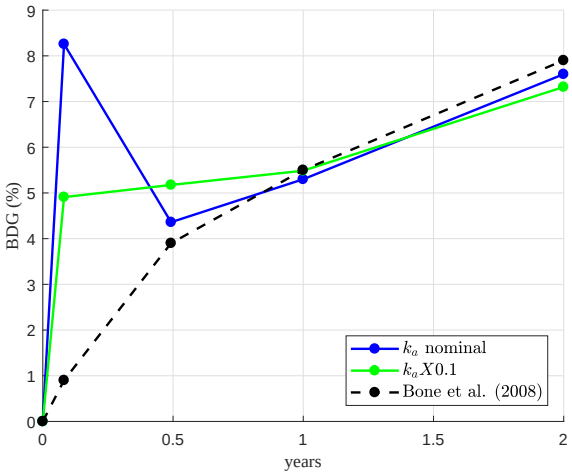

Figure 8: Influence of k_a on BDG for $f_{bm\,t0} = 15\%$.

ical Cases in Mineral and Bone Metabolism 2014;11(3):201–207. URL: http://www.ncbi.nlm.nih.gov/pmc/articles/PMC4269144/.

[2] McClung, M.R.. Denosumab for the treatment of osteoporosis. Osteoporosis and Sarcopenia 2017;3(1):8–17. URL: http://www.sciencedirect.com/science/article/pii/S2405525517300043. doi:https://doi.org/10.1016/j.afos.2017.01.002.

[3] Cummings, S.R., Martin, J.S., McClung, M.R., Siris, E.S., Eastell, R., Reid, I.R.. Denosumab for prevention of fractures in postmenopausal women with osteoporosis. N Engl J Med 2009;361(8):756–765.

[4] Post, T.M., Cremers, S.C.L.M., Kerbusch, T., Danhof, M.. Bone physiology, disease and treatment. Clinical Pharmacokinetics 2010;49(2):89–118. URL: http://dx.doi.org/10.2165/11318150-000000000-00000. doi:10.2165/11318150-000000000-00000.

[5] Recker, R., Lappe, J., Davies, K., Heaney, R.. Remodeling increases substantially in the years after menopause and remains increased

in older osteoporosis patients. Journal of Bone and Mineral Research 2004;19(10):1628–1633.

[6] Riggs, B.L., Parfitt, A.M.. Drugs used to treat osteoporosis: The critical need for a uniform nomenclature based on their action on bone remodeling. Journal of Bone and Mineral Research 2005;20(2):177–184. URL: http://dx.doi.org/10.1359/JBMR.041114. doi:10.1359/JBMR.041114.

[7] Boivin, G., Meunier, P.J.. The degree of mineralization of bone tissue measured by computerized quantitative contact microradiography. Calcified Tissue Int 2002;70(6):503–511.

[8] Bala, Y., Farlay, D., G., B.. Bone mineralization: from tissue to crystal in normal and pathological contexts. Osteoporos Int 2013;24(8):2153–2166.

[9] Post, T.M., Freijer, J.I., DeJongh, J., Danhof, M.. Disease system analysis: Basic disease progression models in degenerative disease. Pharmaceutical Research 2005;22(7):1038–1049. URL: http://dx.doi.org/10.1007/s11095-005-5641-5. doi:10.1007/s11095-005-5641-5.

[10] Marathe, A., Peterson, M.C., Mager, D.E.. Integrated cellular bone homeostasis model for denosumab pharmacodynamics in multiple myeloma patients. Journal of Pharmacology and Experimental Therapeutics 2008;326(2):555–562. URL: http://jpet.aspetjournals.org/content/326/2/555.abstract.

[11] Marathe, D.D., Marathe, A., Mager, D.E.. Integrated model for denosumab and ibandronate pharmacodynamics in postmenopausal women. Biopharmaceutics and Drug Disposition 2011;32(8):471–481. URL: http://dx.doi.org/10.1002/bdd.770. doi:10.1002/bdd.770.

[12] Scheiner, S., Pivonka, P., Smith, D.., Dunstan, C.., Hellmich, C.. Mathematical modeling of postmenopausal osteoporosis and its treatment by the anti-catabolic drug denosumab. International Journal for Numerical Methods in Biomedical Engineering 2014;30(1):1–27. URL: http://dx.doi.org/10.1002/cnm.2584. doi:10.1002/cnm.2584.

[13] Lemaire, V., Tobin, F.L., Greller, L.D., Cho, C.R., Suva, L.J.. Modeling the interactions between osteoblast and osteoclast activities in bone remodeling. Journal of Theoretical Biology 2004;229(3):293–309. URL: http://www.sciencedirect.com/science/article/pii/S0022519304001407. doi:https://doi.org/10.1016/j.jtbi.2004.03.023.

[14] Pivonka, P., Zimak, J., Smith, D.W., Gardiner, B.S., Dunstan, C.R., Sims, N.A., et al. Model structure and control of bone remodeling: A theoretical study. Bone 2008;43(2):249–263. URL: http://dx.doi.org/10.1016/j.bone.2008.03.025. doi:10.1016/j.bone.2008.03.025.

[15] Pivonka, P., Zimak, J., Smith, D.W., Gardiner, B.S., Dunstan, C.R., Sims, N.A., et al. Theoretical investigation of the role of the rankranklopg system in bone remodeling. Journal of Theoretical Biology 2010;262(2):306–316. URL: http://www.sciencedirect.com/science/article/pii/S002251930900441X. doi:https://doi.org/10.1016/j.jtbi.2009.09.021.

[16] Peterson, M.C., Riggs, M.M.. Predicting nonlinear changes in bone mineral density over time using a multiscale systems pharmacology model. CPT: Pharmacometrics and Systems Pharmacology 2012;1(11):1–8. doi:10.1038/psp.2012.15.

[17] Martínez-Reina, J., García-Aznar, J., Domínguez J.and Doblaré, M.. On the role of bone damage in calcium homeostasis. J Ther Biol 2008;254(3):704–712.

[18] Miller, P.D., Bolognese, M.A., Lewiecki, E.M., McClung, M.R., Ding, B., Austin, M., et al. Effect of denosumab on bone density and turnover in postmenopausal women with low bone mass after long-term continued, discontinued, and restarting of therapy: A randomized blinded phase 2 clinical trial. Bone 2008;43(2):222–229. URL: http://dx.doi.org/10.1016/j.bone.2008.04.007. doi:10.1016/j.bone.2008.04.007.

[19] Dua, P., Hawkins, E., van der Graaf, P.H.. A tutorial on target-mediated drug disposition (tmdd) models. CPT: Pharmacometrics and Systems Pharmacology 2015;4(6):324–337. URL: http://dx.doi.org/10.1002/psp4.41. doi:10.1002/psp4.41.

[20] Scheiner, S., Pivonka, P., Hellmich, C.. Coupling systems biology with multiscale mechanics, for computer simulations of bone remodeling. Computer Methods in Applied Mechanics and Engineering 2013;254(1):181–196. URL: http://www.sciencedirect.com/science/article/pii/S0045782512003234. doi:https://doi.org/10.1016/j.cma.2012.10.015.

[21] Pivonka, P., Buenzli P. R. Scheiner, S., Hellmich, C., Dunstan, C.R.. The influence of bone surface availability in bone remodelling - a mathematical model including coupled geometrical and biomechanical regulations of bone cells. Engineering Structures 2013;47(1):134147.

[22] Eriksen, E., Hodgson, S., Eastell, R., Cedel, S., O'Fallon, W., Riggs, B.. Cancellous bone remodeling in type I (postmenopausal) osteoporosis: quantitative assesment of rates of formation, resorption and bone loss at tissue and cellular levels. J Bone Miner Res 1990;5(4):311–319.

[23] Need, A., Horowitz, M., Morris, H., Moore, R., Nordin, C.. Seasonal change in osteoid thickness and mineralization lag time in ambulant patients. J Bone Miner Res 2007;22(5):757–761.

[24] Hernandez, C., Beaupré, G., Carter, D.. A model of mechanobiologic and metabolic influences on bone adaptation. J Rehabil Res Dev 2001;37(2):235–244.

[25] Parfitt, A.. The physiologic and clinical significance of bone hisotomorphometric data. In: Recker, R., editor. Bone Histomorphometry Techniques and Interpretation. Boca Raton, FL, USA: CRC Press; 1983, p. 143–223.

[26] Parfitt, A.. Bone remodeling and bone loss: Understanding the pathophysiology of osteoporosis. Clin Obstet Gynecol 1987;30(4):789–811.

[27] Frost, H.. Bone Remodeling Dynamics. Springfield, IL: Charles C. Thomas Co.; 1963.

[28] Currey, J.. Tensile yield in compact bone is determined by strain, post-yield behaviour by mineral content. J Biomech 2004;37(4):549–556.

[29] Martin, R.. Porosity and specific surface of bone. Crit Rev Biomed Engl 1984;10(3):179–222.

[30] Hernandez, C., Beaupré, G., T.S., K., Carter, D.. The influence of bone volume fraction and ash fraction on bone strength and modulus. Bone 2001;29(1):74–78.

[31] Bone, H., Bolognese, M., Yuen, C., Kendler, D., Wang, H., Liu, Y., et al. Effects of denosumab on bone mineral density and bone turnover in postmenopausal women. J Clin Endocrinol Metab 2008;93:2149–2157.

[32] McClung, M., Harris, S.T., Miller, P.D., Bauer, D.C., Davison, K.S., Dian, L., et al. Bisphosphonate therapy for osteoporosis: Benefits, risks, and drug holiday. The American Journal of Medicine 2013;126(1):13–20. URL: http://dx.doi.org/10.1016/j.amjmed.2012.06.023. doi:10.1016/j.amjmed.2012.06.023.

[33] Anagnostis, P., Paschou, S.A., Mintziori, G., Ceausu, I., Depypere, H., Lambrinoudaki, I., et al. Drug holidays from bisphosphonates and denosumab in postmenopausal osteoporosis: Emas position statement. Maturitas 2017;101:23–30. URL: http://www.sciencedirect.com/science/article/pii/S0378512217305364. doi:https://doi.org/10.1016/j.maturitas.2017.04.008.

[34] Tsourdi, E., Langdahl, B., Cohen-Solal, M., Aubry-Rozier, B., Eriksen, E.F., Guañabens, N., et al. Discontinuation of denosumab therapy for osteoporosis: A systematic review and position statement by ects. Bone 2017;105:11–17. URL: http://www.sciencedirect.com/science/article/pii/S8756328217302673. doi:https://doi.org/10.1016/j.bone.2017.08.003.

Highlights

- Mineralization is an essential mechanism for bone density gain (BDG) after treatment with denosumab.
- Mineralization rate strongly affects the changes in BDG over time. High values lead to earlier saturation.
- The slope of BDG vs. time curves is increased with turnover rate.
- The drug accessibility factor is essential in controlling how denosumab is distributed from the serum to the bone tissue compartment.
- The effect of denosumab on BDG is site specific, being more effective in the lumbar spine than in the hip.

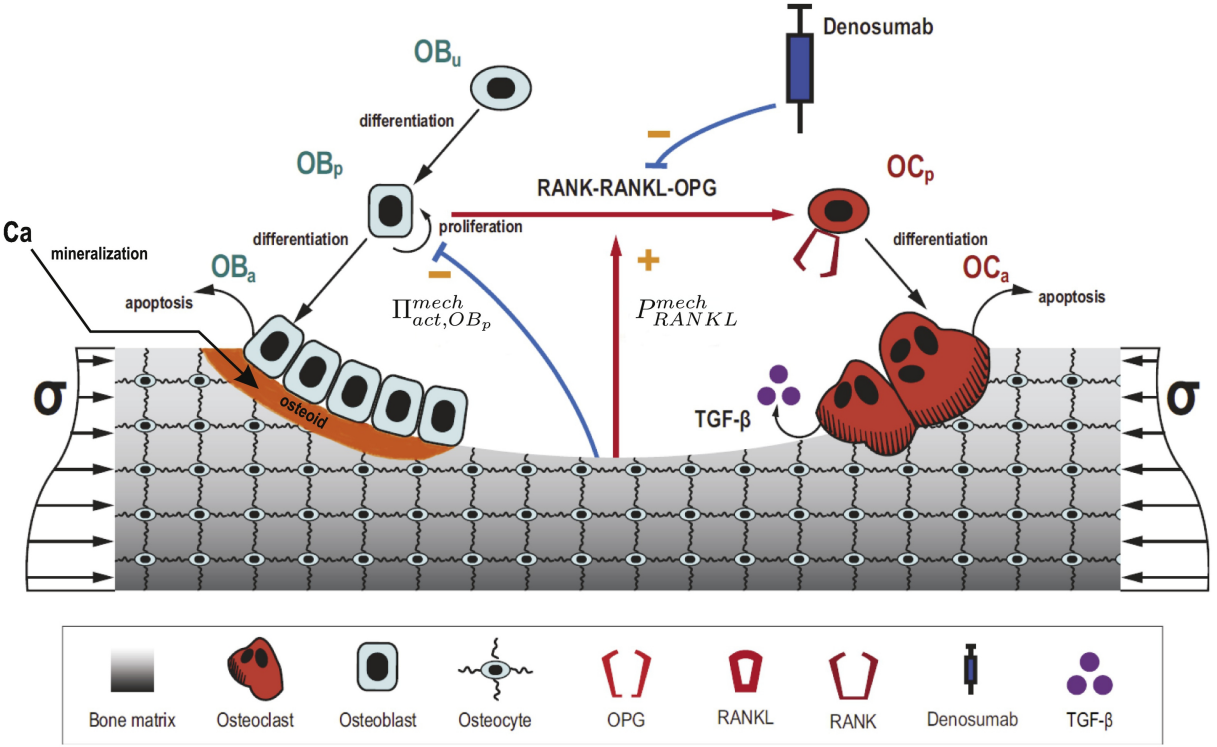
Denosumab
OB_u
differentiation
OB_p
RANK-RANKL-OPG
OC_p
Ca
mineralization
differentiation
proliferation
differentiation
OB_a
apoptosis
Π^{mech}_{act,OB_p}
P^{mech}_{RANKL}
OC_a
apoptosis
σ
osteoid
TGF-β
σ
Bone matrix
Osteoclast
Osteoblast
Osteocyte
OPG
RANKL
RANK
Denosumab
TGF-β

Figure 1

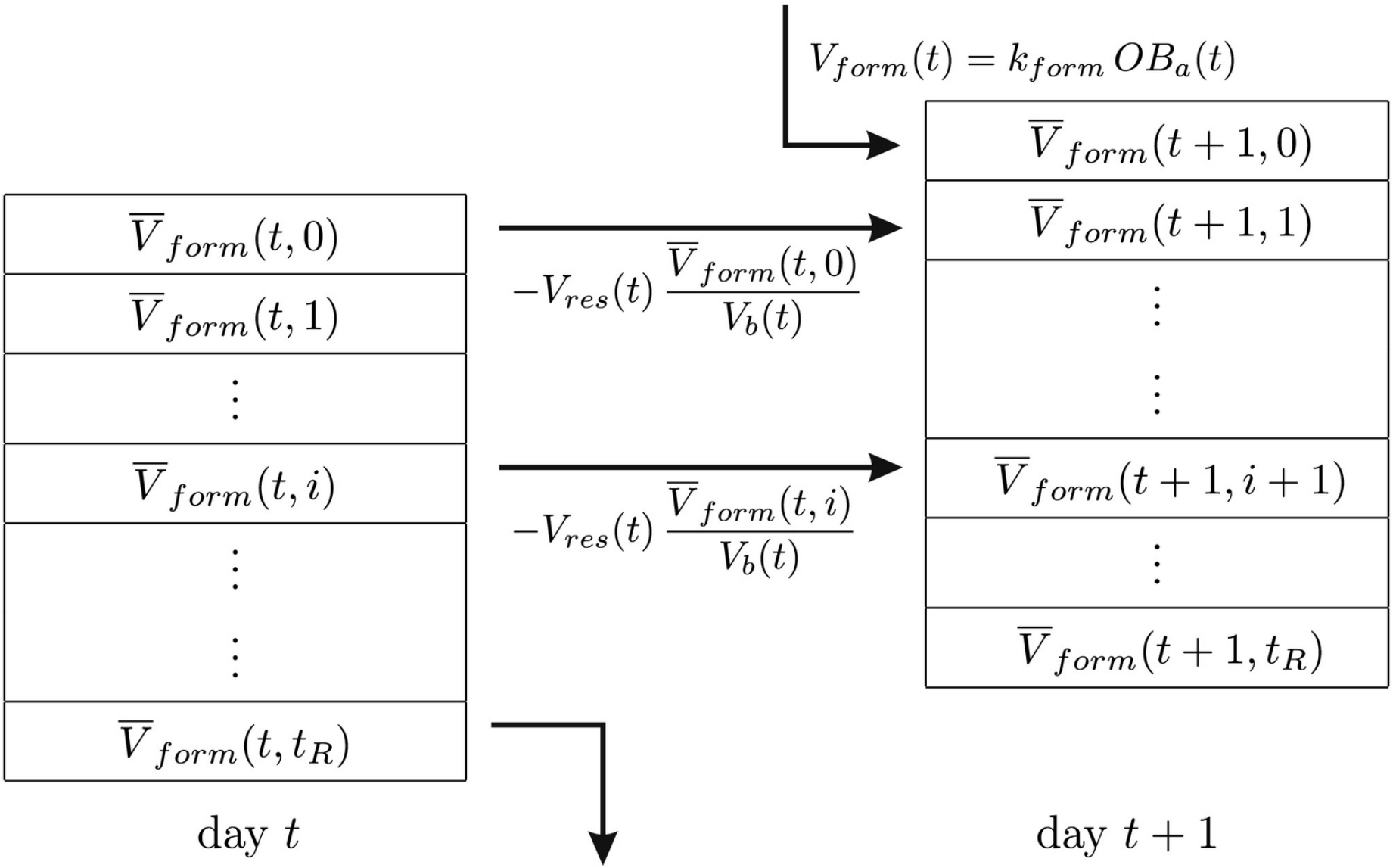
$V_{form}(t) = k_{form}\, OB_a(t)$
$\overline{V}_{form}(t,0)$
$\overline{V}_{form}(t,1)$
$\overline{V}_{form}(t,i)$
$\overline{V}_{form}(t,t_R)$
$-V_{res}(t)\,\dfrac{\overline{V}_{form}(t,0)}{V_b(t)}$
$-V_{res}(t)\,\dfrac{\overline{V}_{form}(t,i)}{V_b(t)}$
$\overline{V}_{form}(t+1,0)$
$\overline{V}_{form}(t+1,1)$
$\overline{V}_{form}(t+1,i+1)$
$\overline{V}_{form}(t+1,t_R)$
day t
day $t+1$

Figure 2

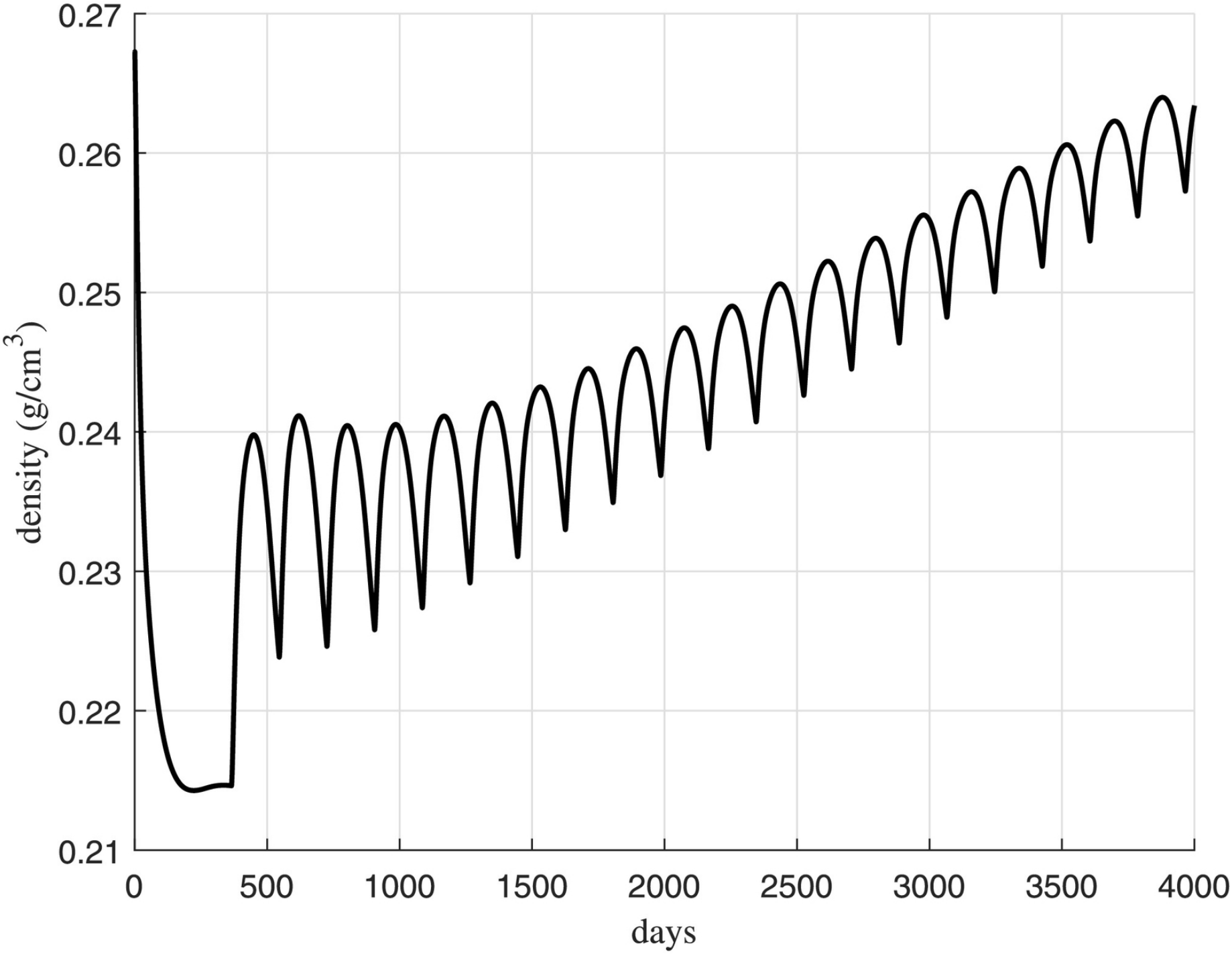
0.27
0.26
0.25
0.24
0.23
0.22
0.21
density (g/cm3)
0
500
1000
1500
2000
2500
3000
3500
4000
days

Figure 3

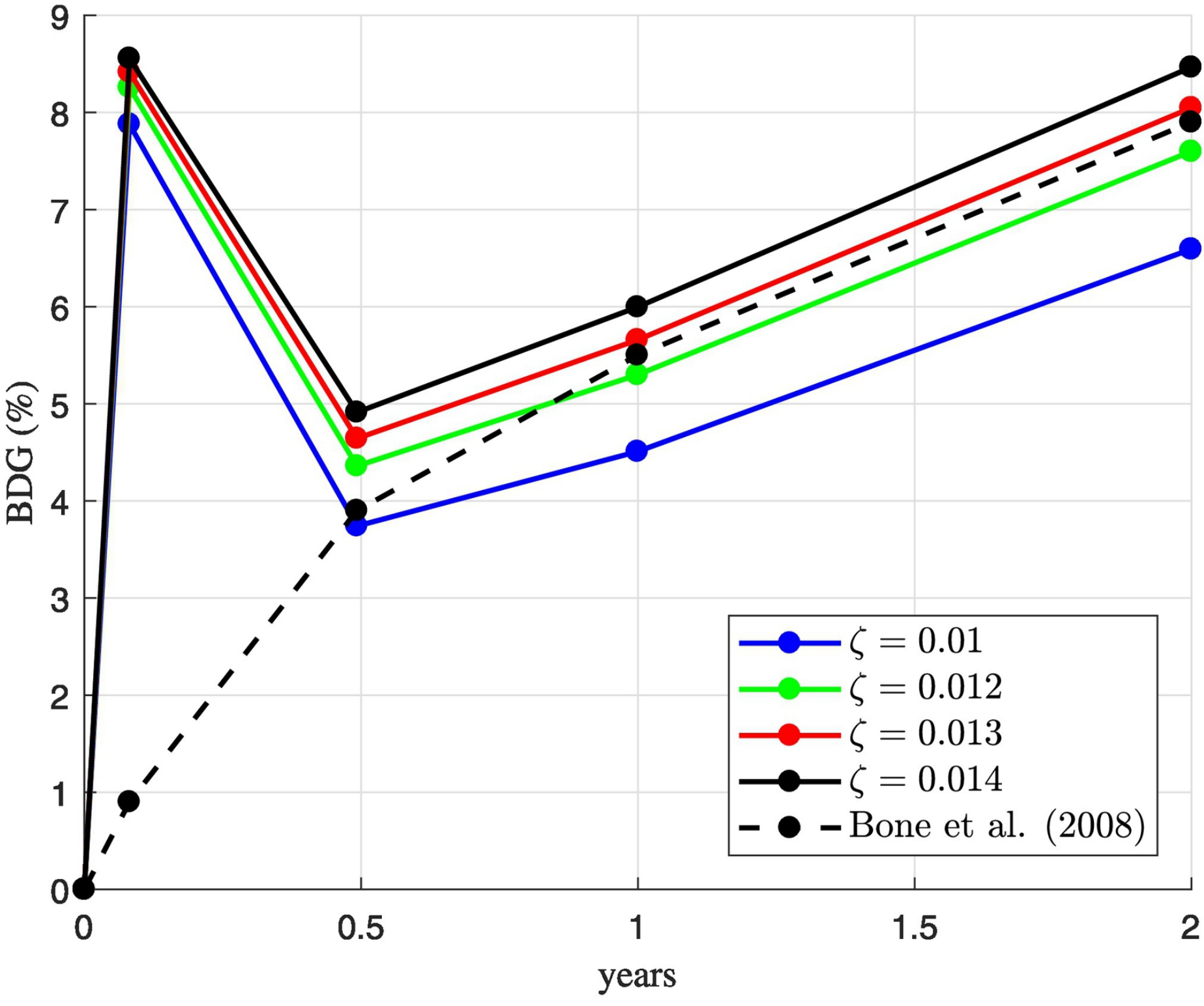
BDG (%)
years
0
1
2
3
4
5
6
7
8
9
0
0.5
1
1.5
2
$\zeta = 0.01$
$\zeta = 0.012$
$\zeta = 0.013$
$\zeta = 0.014$
Bone et al. (2008)

Figure 4

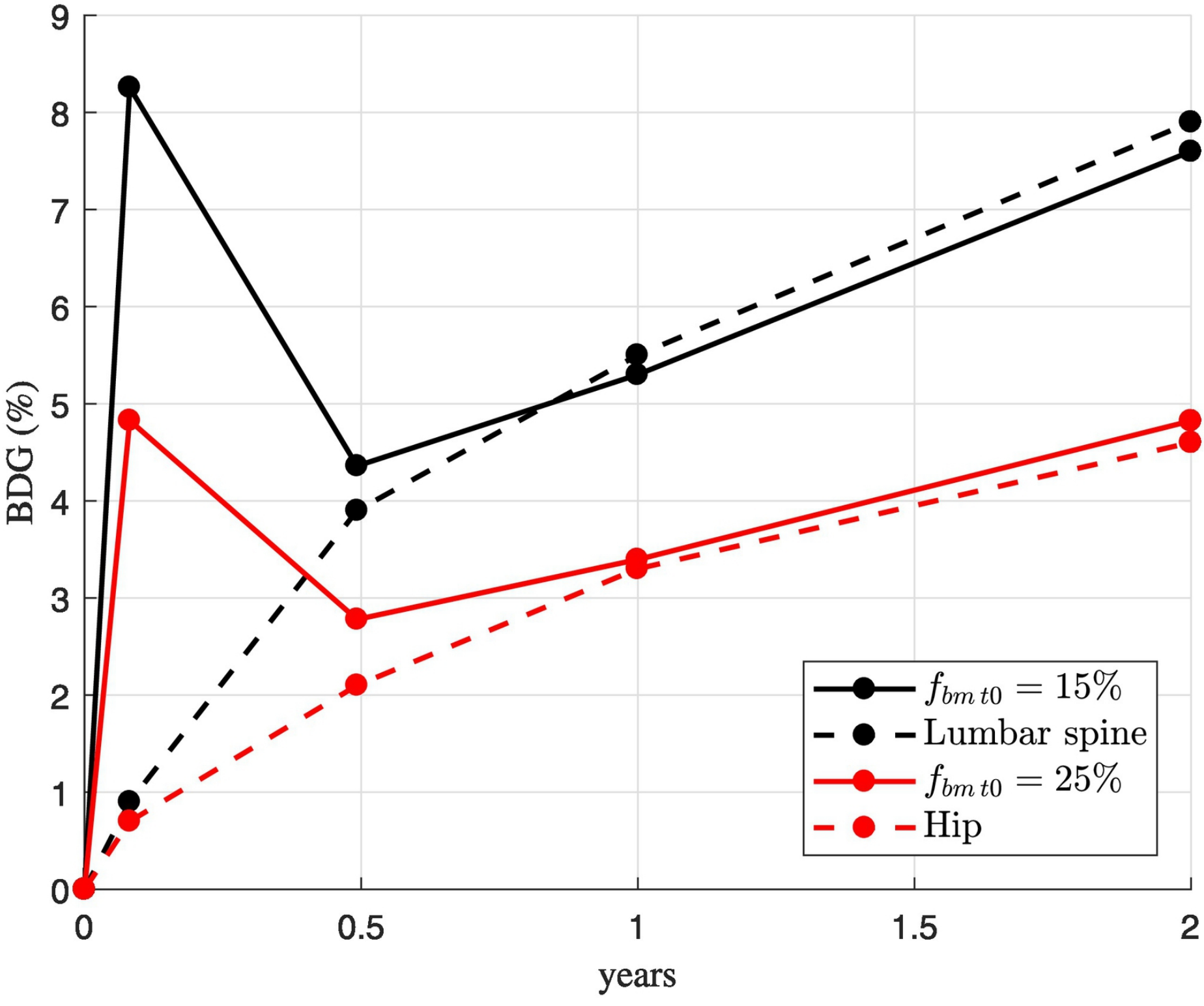
9
8
7
6
5
4
3
2
1
0
BDG (%)
0
0.5
1
1.5
2
years
$f_{bm\,t0} = 15\%$
Lumbar spine
$f_{bm\,t0} = 25\%$
Hip

Figure 5

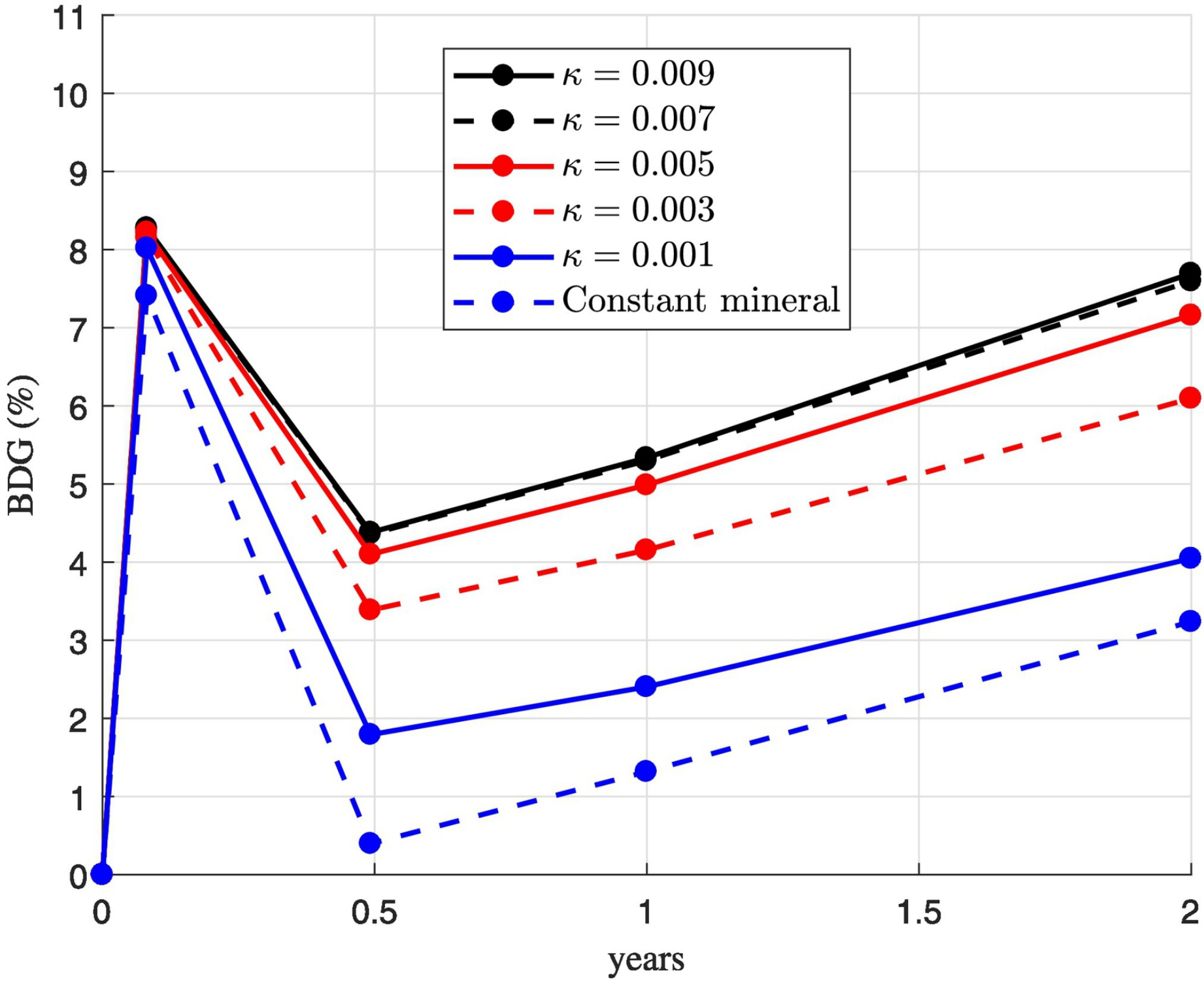
11
10
9
8
7
6
5
4
3
2
1
0
BDG (%)
0
0.5
1
1.5
2
years
$\kappa = 0.009$
$\kappa = 0.007$
$\kappa = 0.005$
$\kappa = 0.003$
$\kappa = 0.001$
Constant mineral

Figure 6

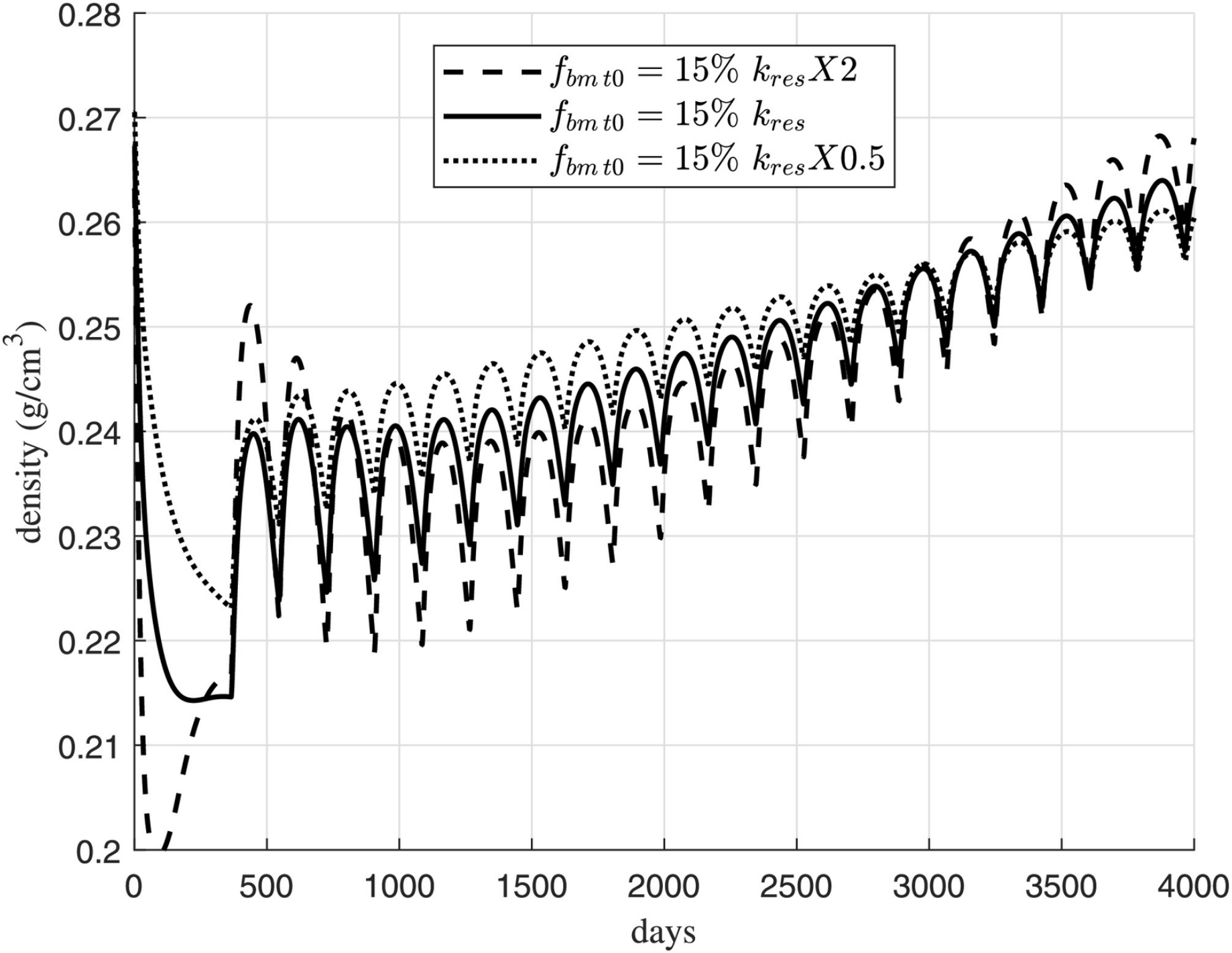
$f_{bm\,t0} = 15\%\ k_{res}X2$
$f_{bm\,t0} = 15\%\ k_{res}$
$f_{bm\,t0} = 15\%\ k_{res}X0.5$
density (g/cm^3)
days
0.28
0.27
0.26
0.25
0.24
0.23
0.22
0.21
0.2
0
500
1000
1500
2000
2500
3000
3500
4000

Figure 7

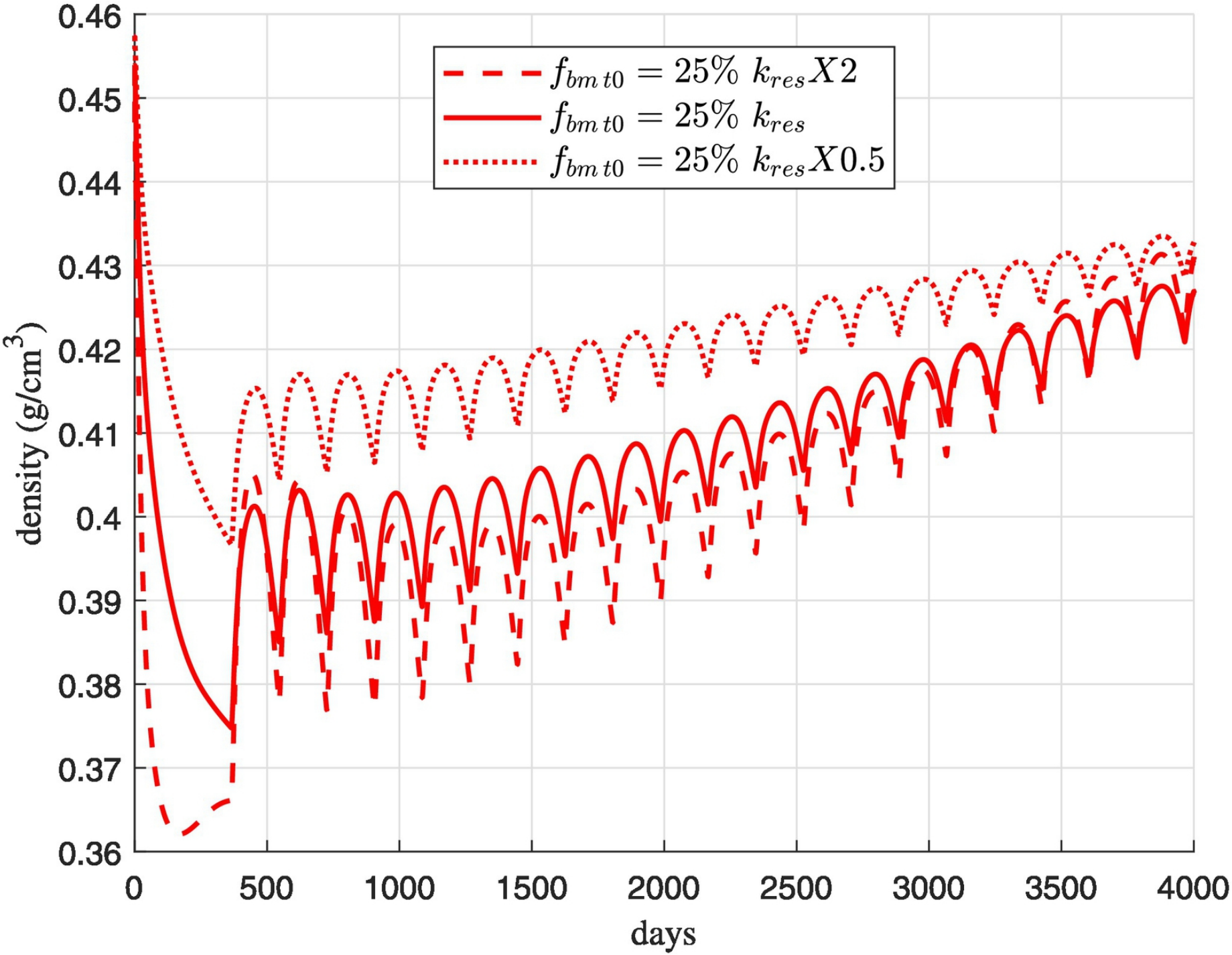
0.46
0.45
0.44
0.43
0.42
0.41
0.4
0.39
0.38
0.37
0.36
density (g/cm^3)
0
500
1000
1500
2000
2500
3000
3500
4000
days
$f_{bm\,t0} = 25\%\ k_{res}X2$
$f_{bm\,t0} = 25\%\ k_{res}$
$f_{bm\,t0} = 25\%\ k_{res}X0.5$

Figure 8

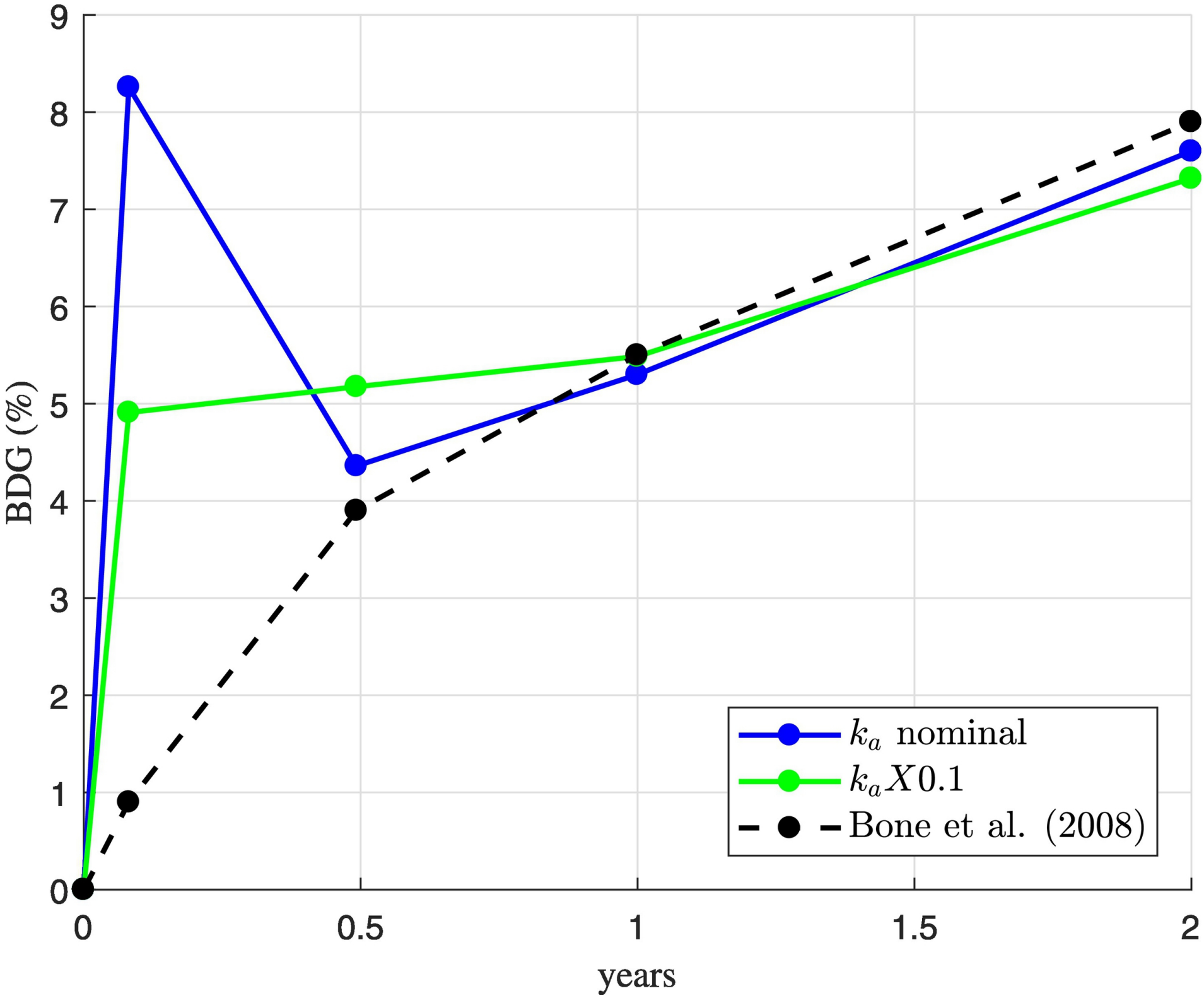
BDG (%)
years
0
1
2
3
4
5
6
7
8
9
0
0.5
1
1.5
2
k_a nominal
$k_a X 0.1$
Bone et al. (2008)

Figure 9